William & Mary

CHARTERED 1693

Undergraduate Honors Theses   Theses, Dissertations, & Master Projects

5-2019

Disentanglement of Whisker Deflection Velocity and Direction

Srijan Bhasin

Follow this and additional works at: https://scholarworks.wm.edu/honorstheses

Part of the Computational Neuroscience Commons

Disentanglement of Whisker Deflection Velocity and Direction
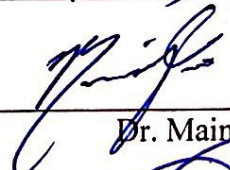
Srijan Bhasin

Department of Mathematics

College of William & Mary

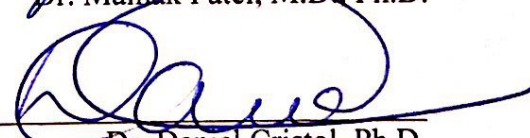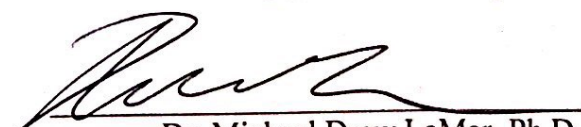Williamsburg, VA 23185, USA

May 1, 2019

Accepted for __Honors_____

_____
Dr. Mainak Patel, M.D., Ph.D.

_____
Dr. Daniel Cristol, Ph.D.

_____
Dr. Michael Drew LaMar, Ph.D.

Abstract

The easily identifiable structure and clearly defined function of the rodent somatosensory barrel cortex has made it a model system for study in neuroscience. The barrel consists of ~3600 regular-spiking (RS) cells that receive inhibitory inputs from <400 fast-spiking (FS) cells, both of which are excited by ~240 thalamocortical (TC) cells. RS cell population dynamics such as rate of spiking and region of increased spiking can encode velocity and directional information from the initial whisker deflection, however, behavior of any single RS cell (or small group of RS cells) may be ambiguously affected by both velocity and directional changes. This project set out to create an additional layer of RS-like cells, hereby referred to as "excitatory extensions," whose individual behavior or small group dynamics can correctly classify velocity and directional information from the incoming input stimulus. The model shows that an architecture that takes advantage of the net scaling of RS cell layer activity can lead to EE cells that correctly classify velocity without dependency on directional input. The model also shows that an architecture that engages an inhibitory feedback system can lead to EE cells that correctly classify direction without dependency on velocity input. Further areas of study include putting two barrel systems in communication with one another while limiting the model to experimentally-supported cell dynamics to see if architecture similar to the ones discovered in this project arise.

Acknowledgments

Introduction

Since its discovery in the early 1970s, researchers have used the rodent barrel cortex as a model system in neuroscience. Its easily identifiable structure allows scientists to relate form to function, thus lending itself to questions relating to cortex development, neuronal plasticity, and active touch, among others. The barrel cortex is the most overrepresented part of the somatosensory cortex, occupying roughly 70% of it, for a total of 13% of total cortical area (Fox, 2008). The cortex is a six-layered structure, with each layer comprised of distinct populations of cells. Layer IV has the highest density of neurons and is the main recipient of the thalamic axons that encode the tactile information from rodent whiskers (Beaulieu, 1993). Neurons of layer IV are arranged into discrete multicellular units called barrels that are dedicated to processing sensory information from a single whisker. Each barrel consists of roughly 3,600 excitatory regular-spiking (RS) cells and 400 inhibitory fast-spiking (FS) cells that provide time-lagged inhibition to RS cells (Beaulieu, 1993; Sun et al, 2006.; Kawaguchi and Kubota, 1993). Barrel fields are areas that consist of all barrels associated with whiskers on one side of the animal (up to 220) and have a consistent topological map that is defined by the physical arrangement of whiskers on the rodent itself, shown in Figure 1 (Woolsey and Van der Loos, 1970; Woolsey and Welker, 1974; Petersen, 2007). Barrel fields have consistent appearances from hemisphere to hemisphere (Woolsey and Welker, 1974).

Experiments in anesthetized animals show that the barrel system processes information relating to velocity and angular direction of deflection (Bale and Maravall, 2018). This information is initially sensed through the whisker bending moment that provides the major drive for primary mechanosensory cells (Peron et al., 2015; Campagner et al., 2016). The encoding of the bending moment is proportional to deflection angle and the temporal derivative of the

bending moment is proportional to deflection velocity (Campagner et al., 2018). This information is then transferred to thalamic barreloids, which process it and send it to the cortex barrel. Barreloids contain 240 – 300 thalamocortical (TC) neurons, whose axons converge on the cortical barrels of the same corresponding whisker (Keller and Carlson, 1999). Thus, a functional unit to interpret sensory information consisting of whisker, barrel, and barreloid is formed. Up to 5% of the barreloid's axons terminate in the hollow of a cortical barrel that is adjacent to the corresponding barrel (Land et. al., 1995).
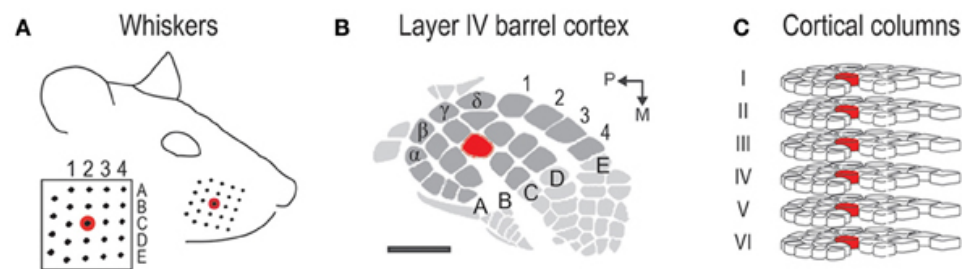

Figure 1: (A) Spatial orientation of the largest 24 whiskers with grid-naming convention. Whisker C2 is highlighted in red. (B) Spatial orientation of barrels (shaded in dark grey) within layer IV of the primary somatosensory cortex. Topological orientation of whiskers is maintained, thus allowing for the same grid-naming convention to be employed. Barrel corresponding to whisker C2 is highlighted in red. (C) Cortical columns for the same 24 whiskers. Each column contains neurons that respond preferentially to a particular whisker. Neurons responding to whisker C2 are highlighted in red (Chen-Bee et al., 2012)

TC excitatory cells synapse onto both FS and RS cells and their excitatory post-synaptic potential (EPSP) strength varies based on target cell. Axons from the thalamus make stronger and more frequent connections onto FS cells than RS cells, thus eliciting reliable and precisely timed action potentials within FS neurons (Sun et al., 2006; Cruikshank et al., 2007). If thalamocortical excitatory currents rise quickly, RS cells may fire action potentials before significant inhibition arrives. However, if thalamocortical currents rise slowly in excitatory cells, an overlapping with feedforward inhibitory currents may suppress action potentials. Therefore, a

system of robust detection of synchrony among the input cells (TC cells) is formed (Bruno, 2011; Joshi and Patel, 2013; Patel and Joshi, 2013). This type of feed forward inhibitory architecture, shown in Figure 2, is found in a number of neural systems, including the locust olfactory system, the rodent hippocampus, and the rodent auditory system, among other (Leitch and Laurent, 1996; Deng and Rogers, 1998; Fricker and Miles, 2000; Pouille and Scanziani, 2001; Sridharan et al., 2011; Perez-Orive et al., 2002; Wehr and Zador, 2003; Benowitz and Karten, 2004; Blitz and Regehr, 2005; Mittmann et al., 2005; Jortner et al., 2007; Patel and Reed, 2013).
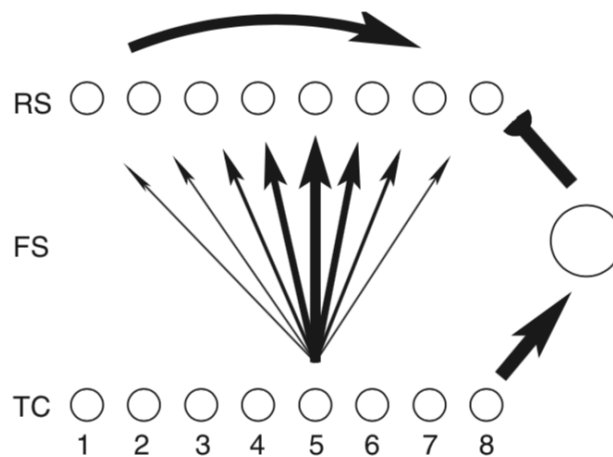
Figure 2: Schematic of the barrel model. Arrow heads indicate excitation; semicircular heads indicate inhibition. TC and RS cells are split into 8 directional groups, with the density of TC to RS synapses shown by thickness of the arrow. TC cells show a connection preference for RS cells directly aligned with their directional preference. Connectivity is analogous for TC direction groups 1-4 and 6-8. Lateral RS-to-RS connections have a probability of 0.2.

Schematic also shows architecture needed for phase-delayed inhibition. A set of excitatory encoder cells (TC cells) synapse onto both a set of inhibitory interneurons (FS cells) and decoder neurons (RS cells). The decoder neurons also receive input from the inhibitory interneuron. Each excitatory TC group spike is followed by an inhibitory interneuron spike after a short, relatively constant time delay (Patel, 2018).

The TC barreloid encodes angular deflection direction and deflection for its corresponding whisker. TC cells within the barreloid have directional preferences and cells with

like angular preference are physically clustered within the barreloid (Timofeeva et al., 2003).

The magnitude of spike response of any given TC direction group diminishes as angular direction of whisker deflection deviates from the preferred direction toward the opposite direction, 180º away. However, the net spiking activity of the barreloid system as a whole, accounting for the spiking of every directional group, remains roughly constant for each deflection direction (Pinto et al., 2000; Bruno and Simons, 2002; Temereanca and Simons, 2003). Deflection velocity is encoded within a barreloid by spike synchrony. Different deflection velocities lead to similar net spike counts within the barreloid, however, synchrony of TC cell spikes increases with velocity (Pinto et al., 2000; Bruno and Sakmann, 2004; Temereanca et al., 2008). Thus, within the barreloid, changing deflection direction alters the physical distribution of the spike counts across the TC groups (without altering net barreloid spike count), while changing velocity alters synchrony of TC cell spikes (again, without altering net barreloid spike count).

Within the barrel, FS cells are selective for neither direction nor velocity, providing strong inhibitory currents to RS cells for all whisker deflection velocities (Lee and Simons, 2004) and directions (Simons and Carvell, 1989). Barrel RS cells exhibit both velocity and direction tuning. Experimentally, it has been shown that the directional tuning of an RS cell sharpens as the velocity of deflection decreases (Lee and Simons, 2004).

Velocity tuning of RS cells is thought to arise from the feed-forward inhibition circuitry of the barreloid-barrel system. High deflection velocities lead to highly synchronized TC cell spikes. These spikes provide EPSPs to the RS cell within a short time window, before the arrival of the strong inhibitory post-synaptic potential (IPSP) from the FS cell. This leads to a high probability of spiking within the temporal window of unopposed excitation. As deflection

velocities decrease, TC spikes desynchronize, hence fewer EPSPs impinge upon the RS cell prior to the arrival of the powerful IPSP from FS cells. Ultimately, this leads to a lower probability of an RS cell spike (Pinto et al. 2000; Temereanca and Simons, 2003; Bruno and Sakmann, 2004; Cruikshank et al., 2007; Temereanca et al., 2008; Liu et al., 2014).

RS cell direction selectivity is less clear. RS cells within the barrel are clustered into domains based on angular preference corresponding to groups within the thalamus (Pinto et al., 2000). However, terminals of a TC axon disperse widely throughout all RS direction domains in the corresponding barrel, though density of connections rises as the directional preference of the RS group and TC group more closely align (Bruno and Simons, 2002; Bruno et al.; Timofeeva et al., 2003; Furuta et al., 2011). Wilent and Contreras showed in their 2005 study that the peak values for net excitatory and inhibitory input to a cell change little as the direction of a whisker deflection deviates away from the preferred. However, the timing of the peak in net excitatory input shifts, thus approaching the fixed time peak of the net inhibitory input from FS cells. A large-scale model of the barrel-barreloid system showed that RS-RS excitatory synapses can naturally account for the unexplained directional dependence of RS cell inputs. As deflection direction deviates away from the preferred direction of an RS cell, TC input declines, but RS-RS synaptic transmission buffers the decline in net excitatory input. However, this causes a shift in the timing of the excitatory input peak from the peak in the TC input to the delayed peak in the RS input (Patel, 2018).

Although single RS cell spikes are ambiguous in their relationship to stimulus velocity or direction, the entire barrel RS population does exhibit velocity and direction tuned responses. The spike response of an individual RS cell diminishes both as deflection velocity decreases and as deflection direction deviates away from the preferred direction (leading to ambiguity about the

cause of said response changes) (Pinto et al., 2000; Bruno and Simons, 2002; Lee and Simons, 2004; Wilent and Contreras, 2005). However, as velocity increases, TC cell synchrony leads to a net increase in barrel RS cell spikes. Hence, the synchrony code used by TC cells contains the same information as the rate code used by RS cells (the temporal precision of RS cell spikes remains relatively constant across velocities). And, the rate code employed by TC directional groups to encode deflection direction is preserved in the activity of directional group activity of RS cells (Pinto et al., 2000; Bruno and Sakmann, 2006; Temereanca et al., 2008).

The purpose of this project was to develop a model cell that disentangles velocity and direction information from the population activity of the RS neurons. This represents a biological need for animals, as whiskers act as a main sensory tool (Fox, 2008). Animals must be able to pinpoint direction (independent of velocity) and velocity (independent of direction) and continue to interpret this information past the barrel system in order to understand and react to their physical environment. I developed a biologically detailed model of a single barrel/barreloid system responding to a single whisker that incorporates realistic network connectivity and synaptic dynamics. I showed that the model captures experimental dynamics of direction and velocity response and then extended the model by adding an additional layer of neurons that spiked in response to a specific direction, regardless of velocity of deflection, or in response to a specific velocity, regardless of direction of deflection. Although there is no biological evidence that such cells exist, this speculative study shows potential mechanism that may appear in the true biological mechanism.

Methods:

As shown in Figure 2, the base model consists of three cell populations: a thalamocortical (TC) cell population, a set of inhibitory fast-spiking (FS) cortical cells, and a set of excitatory regular-spiking (RS) cortical cells that receive input from the TC and FS populations. Connections among neurons are random but fixed, with defined direction- and cell type- specific connection probabilities.

Stimulus Modeling:

As observed experimentally (Land et al., 1995), the model barreloid consists of 240 TC cells. Because TC cells show clustering by directional preference (Timofeeva et al., 2003), TC cells in the model are split into 8 direction groups of 30 cells each. Each group is assigned a preferred whisker deflection direction (0º, ± 45º, ± 90º, ± 135º, 180º) away from arbitrary simulated whisker deflection. Experimental data indicate that a whisker deflection tends to elicit at most one spike in a TC cell (Pinto et al., 2000). Therefore, TC cells are assigned spike probabilities (each TC cell spikes 0 or 1 times over the course of the simulation) and spike times are drawn for those cells that did spike. Spike times are drawn from an inverse Gaussian distribution, which has shown to be the most concordant in shape with experimentally measured TC spike time distributions (Pinto et al., 2000).

Within a barreloid, experiments show that different whisker deflection velocities lead to similar net spike counts, however, the synchrony of TC cell spikes is altered (Pinto et al., 2000; Bruno and Sakmann, 2006; Temereanca et al., 2008). To simulate encoding of velocity via spike synchrony, higher whisker deflection velocities decreases the standard deviation of the TC spike time distribution in the model, while leaving spike probabilities for the population unchanged.

To simulate lower deflection velocities, the standard deviation is increased, again, while leaving spike probabilities for the population unchanged. The TC spike time distribution has a set mean of 10 ms, and the six velocities are simulated by setting the standard deviation of the distribution to [1, 1.25, 1.5, 2, 2.5, or 3] * ms (listed from highest to lowest velocity). In manuscript figures, the inverse of the standard deviation of the TC spike time distribution is used as a stand-in for stimulus deflection velocity.

Experimental data also show that TC cells are clustered into groups based on direction preference (Timofeeva et al., 2003) and that as direction of deflection deviates away from the preferred direction of a group, the magnitude of the group's response is lessened. However, the synchrony of the TC group's response does not change noticeably (Pinto et al., 2000; Temereanca and Simons, 2003). To simulate encoding of direction via response magnitude, TC spike probability within a given direction group was set at [0.8, 0.7, 0.4, 0.15, 0.1] to simulate a whisker deflection at a direction of [$0°$, $\pm 45°$, $\pm 90°$, $\pm 135°$, $180°$], respectively, away from the preferred direction. This leads to a tuning ratio (response to preferred direction/average response over all directions) of 1.86 for individual TC cells. This is concordant with the experimental tuning ratio of 1.8 shown in Bruno and Simons (2002). Thus, stimulus velocity is encoded by standard deviation of the TC spike time distribution while stimulus direction is encoded for by varying spike probabilities for directional groups within the barreloid.

Model Equations:

Although TC cells are not explicitly simulated, RS, FS, and both excitatory and inhibitory extension cells are modeled by the reduced dimensional integrate-and-fire model of a cortical cell below:

Equation (1):

$$\frac{dV^{k,j}}{dt} = -g(V^{k,j} - V_{rest}) + I^{k,j}(t)$$

where k∈{fs, rs}, while j ∈ {1, 2, …, 100} for k = fs and j ∈ {1, 2, …, 800} for k = rs. The non-dimensional membrane potential, $V^{k,j}$, ranges from 0 to 1. The resting membrane potential, V_{rest}, is set to zero. A spike is recorded when the membrane potential value reaches 1 from below. At the first time step when $V^{k,j} \geq 1$ (the membrane potential reaches 1 from below), a neuron spike is recorded and the membrane potential is held at the resting potential for 2.0ms, the length of the refractory period. When a presynaptic neuron spikes, all postsynaptic cells receive a current following a defined latency period. $g = 0.05\text{ms}^{-1}$ is the leak conductance. This term causes a slow leak current that returns the membrane potential to zero. The integrate-and-fire equation has a membrane time constant of 20ms, roughly equal to the experimentally observed value of 17ms in RS cells (Gabernet et al., 2005). This model of the neuron is based on a non-dimensionalized model of neurons of the visual cortex (Tao et al., 2004).

A spike of a neuron presynaptic to k, j leads to a jump in $I^{k,j}(t)$ followed by exponential decay. There is a manually imposed synaptic delay period that is defined for each synapse type. If the rth presynaptic spike occurs at time $t_r^{k,j}$ and m∈{tc, fs, rs} is the type of presynaptic neuron, the current $I^{k,j}$ induced in neuron k, j at time t is given by the following:

Equation (2):

$$i_r^{k,j} = \begin{cases} 0 & t < t_r^{k,j} + d_m^k \\ A_m^k e^{-a_m^k(t - t_r^{k,j} - d_m^k)} & t \geq t_r^{k,j} + d_m^k \end{cases}$$

Equation (3):

$$I^{k,j}(t) = \sum_{r=1}^{n^{k,j}} i_r^{k,j}(t)$$

d_m^k denotes the synaptic delay, a_m^k dictates the decay rate of the current, and A_m^k indicates the amplitude of an input from neuron of type m∈{tc, fs, rs} to a neuron of type k∈{fs, rs}. For the synaptic delay, $d_{tc}^{fs} = d_{tc}^{rs} = d_{fs}^{fs} = 0$ and $d_{fs}^{rs} = d_{rs}^{rs} = 2\ ms$. Introducing the delay parameter was necessary to force the experimentally observed ~2ms time lag between when the EPSP of a TC spike and the IPSP of an FS spike reach an RS cell. The decay rate values are as follows: $a_{tc}^{fs} = 0.73, a_{tc}^{rs} = 0.75, a_{fs}^{fs} = 0.18, a_{fs}^{rs} = 0.18$, and $a_{rs}^{rs} = 0.24$ ms⁻¹. These values approximately match experimental data that show TC synapses to be fast, decaying over a 1-2ms time scale, while FS synapses are slower, decaying over a 5-6ms time scale (Gabernet et al., 2005). The amplitude values are as follows: $A_{tc}^{fs} = 0.3, A_{tc}^{rs} = 0.06, A_{fs}^{fs} = 0.1, A_{fs}^{rs} = 0.03$, and $A_{rs}^{rs} = 0.008$ ms⁻¹. The amplitude parameters allow for agreement with the following experimental observations: (1) TC spikes elicit a ~4-8 fold larger EPSP in an FS cell than an RS cell (Cruikshank et al., 2007) and (2) the postsynaptic current in an RS cell induced by a whisker deflection is dominated by inhibition (in an RS cell the ratio $\frac{EPSC}{EPSC+IPSC} = $ ~0.2) (Gabernet et al., 2005). RS-RS cell synapses have not been characterized experimentally and are assumed to be fast.

Model Connectivity:

The model consists of 240 TC cells, 100 FS cells, and 800 RS cells. RS cells are slip into 8 directional groups of 100 cells each, with each group corresponding to a TC direction group.

FS cells have been shown to respond strongly to all deflection directions (Simons and Carvell, 1989; Bruno and Simons, 2002; Lee and Simons, 2004). Therefore, it is likely that TC input to FS cells is also not direction selective (Swadlow and Gusev, 2002); hence, the TC → FS connection probability is set to 0.65 for all TC direction groups (Bruno and Simons, 2002). Experimentally, the connection probability of TC → RS cells has been estimated to be ~0.37 on average, with each RS cell receiving input from 80-90 TC cells (Bruno and Simons, 2002; Timofeeva et al., 2003; Bruno and Sakmann, 2006; Furuta et al., 2011). Experiments have also shown that TC cell axons arborize throughout the whole barrel, with the highest density of axons staying within a ~200μm horizontal range (Jensen and Killackey, 1987; Arnold et al., 2001). An RS direction domain within the barrel has a horizontal span of ~100μm, and individual RS cell dendritic arbors span ~200μm (Keller and Carlson, 1999; Bruno and Simons, 2002; Bruno et al. 2003; Lubke et al., 2000). Thus, it can be assumed that the a TC cell makes widespread synaptic connections to RS cells throughout the barrel, while the likelihood of a TC → RS connection varies in a direction group dependent manner. Higher connection probabilities can be associated with greater alignment between RS and TC direction group preference. Using this information, the connection probabilities for a TC direction group to an RS direction domain is set at 0.7, 0.5, 0.3, 0.15, and 0.1 for TC group-RS domain alignments that vary by 0º, ± 45º, ± 90º, ± 135º, 180º, respectively. This leads to an average TC → RS connection probability of 0.35, with ~84 TC cells synapsing onto an RS cell (Patel, 2018).

The FS → FS connection probability is set to 0.5. This sets up an architecture that curtails the stimulus-induced FS population response. The FS → RS connection probability is set to 1 as these connections simply serve to provide potent inhibition after a time lag. Experiments indicate that RS → RS synapses are likely to be numerous (Benshalom and White, 1986; Lubke

et al., 2000) and widespread (considering the ~200μm span of dendritic arbors). Therefore, the model includes a connection probability of 0.2, causing an average of 160 presynaptic RS cells to each RS cell.

To disentangle velocity information from directional information, a layer consisting of 6 "Excitatory Extension (EE)" cells is added on top of the RS cells. Each EE cell is arbitrarily assigned a velocity to which it is specific. This layer receives stimulus from RS cells and other EE cells. The RS $\rightarrow$ EE probability is set to 0.2 for every RS directional group to each of the EE cells (leading to an average of 160 presynaptic RS cells to each EE cell). The amplitude $A_{rs}^{ee} = 0.04$, decay rate $a_{rs}^{ee} = 0.24$, and $d_{rs}^{ee} = 0$. EE cells provide inhibition to all EE cells that correspond to velocities lower than that of the presynaptic neuron. These synapses are characterized by $A_{ee}^{ee} = 0.2$, decay rate $a_{ee}^{ee} = 0.18$, and $d_{ee}^{ee} = 0$.

To disentangle direction information from velocity information, a layer consisting of 8 EE cells is added on top of the RS cells. Another layer of 8 "Inhibitory Extension (IE)" cells is then added over the EE cell layer. The EE and IE cells are assigned a direction corresponding to the TC groups. The RS $\rightarrow$ EE probability is set to 0.2 for every RS directional group to each of the EE cells (leading to an average of 160 presynaptic RS cells to each EE cell. The amplitude, however, varies based on difference in directional preference of the presynaptic RS cell and the post-synaptic EE cell. For directional differences of $[0º, \pm 45º, \pm 90º, \pm 135º, 180º]$, $A_{rs}^{ee} = [0.018, 0.014, 0.011, 0.005, 0.003]$. Decay rate $a_{rs}^{ee} = 0.18$, and $d_{rs}^{ee} = 0$. The connection probability for EE $\rightarrow$ IE cells with the same directional preference is set to p = 1, while the connection for any other directional preference is set to p = 0. These synapses are characterized by $A_{ee}^{ie} = 0.5$, decay rate $a_{ee}^{ie} = 0.18$, and $d_{ee}^{ie} = 0$. IE $\rightarrow$ EE synapse probability is set to p = 0

for the cell of the same directional preference and p = 1 for the cells of differing preferences.

These inhibitory synapses are characterized by $A_{ie}^{ee} = 0.5$, decay rate $a_{ie}^{ee} = 0.18$, and $d_{ie}^{ee} = 1$.

Simulation:

The simulation, written in Python, runs with a 0.1ms time step. At each time step, each neuron's synaptic input is calculated. The Euler method is used to analytically solve the membrane equation. All data presented in manuscript figures are averaged over 100 trials. At the end of the simulation, data are processed using SciPy and NumPy packages in Python.

Results and Discussion

Base Model:

Figure 3A shows the membrane potential and input current to a sample RS cell in response to simulated deflection aligned with the cell's preference and in the opposite direction (180° away). Figure 3B shows the corresponding raster plots for the single trial spike. As direction varies from preferred to opposite, the temporal distribution of TC-input current does not change. However, the peak magnitude of the incoming current is decreased. This can be explained by the mechanisms through which TC cells encode direction information. The probability that a TC cell spikes is decreased as its directional domain strays farther from the direction of the incoming stimulus. The TC spike time distribution, however, remains fixed. As TC and RS group directional preference more closely aligns, TC→RS connection probability increases. Thus, an RS cell receives more net TC spikes, and thus net TC current, for a stimulus aligned with its directional preference than for a stimulus straying from the preference. This also explains why the total number of spiking RS in a particular group decreases as the stimulus

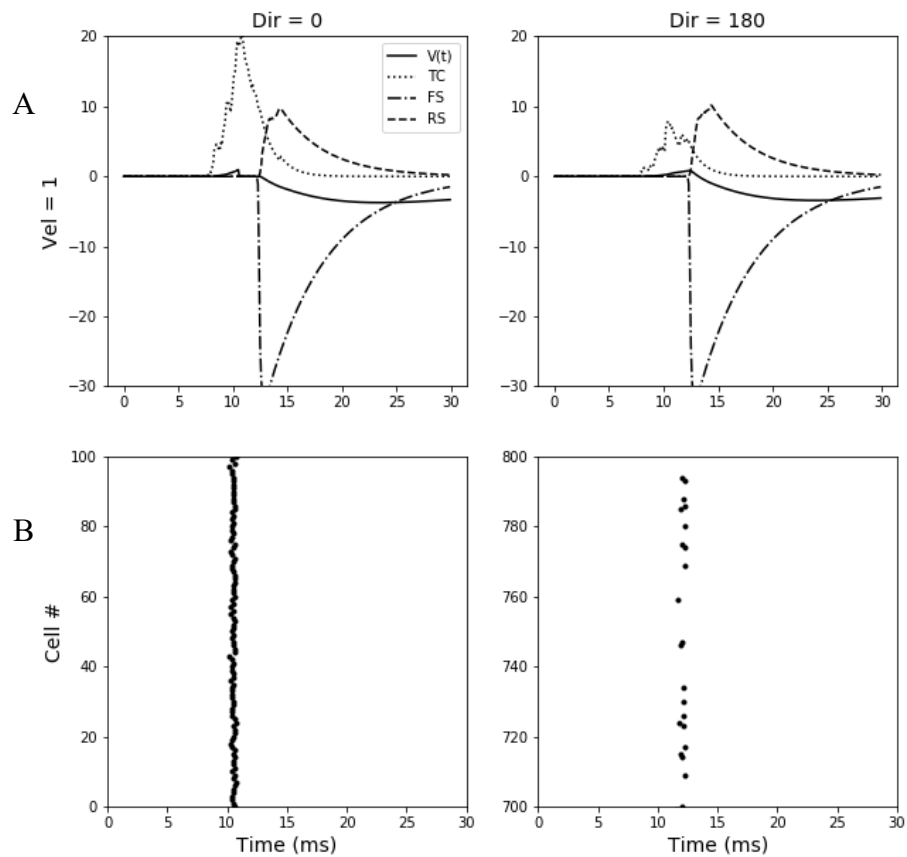direction varies toward 180º away from preference.

Figure 3: Sample RS cell behavior and single-stimulus raster plots. Stimulus velocity is fixed at 1 (inverse of the standard deviation of the TC cell spike time distribution is used to represent deflection velocity in figures). (A) Single trial plots tracing membrane potential, TC excitatory input, RS excitatory input, and FS inhibitory input for a cell within the 0º (left) and 180º (right) directional domains. (B) Single spike raster plots of all cells within the 0º direction domain (left) and 180º direction domain (right) for corresponding trials.

Figure 4A and 4B again show the membrane potential and input current to a sample RS cell and corresponding raster plots for the single trial spikes. Comparing Figures 3 and 4 allows for a qualitative analysis of the effects of decreased velocities. As velocity decreases, the temporal distribution of TC input is broadened, however the time integral of the curve is unaltered. This can be explained by TC cells' encoding of velocity information. As velocity decreases, TC cell spiking becomes less synchronous, but the net number of spikes from every directional group is unchanged. Net RS cell spiking throughout the barrel becomes less

synchronous as a result of the longer time period over which excitatory current is coming in.

This broadened TC excitatory input also overlaps more heavily with the incoming FS inhibitory

input. If a particular RS cell does not reach threshold before receiving the strong inhibitory

current, it is unlikely to fire. Thus, the net RS cell spiking throughout the barrel also becomes
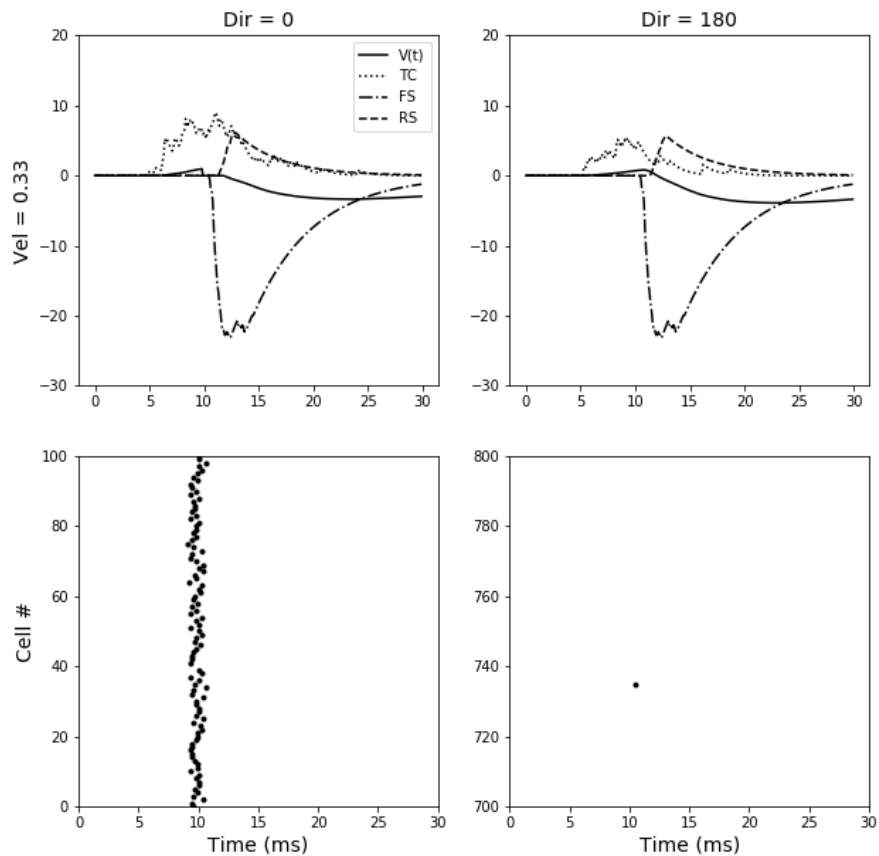
less abundant as velocity decreases.

Figure 4: Sample RS cell behavior and single-stimulus raster plots. Stimulus velocity is fixed at 0.33 (inverse of the standard deviation of the TC cell spike time distribution is used to represent deflection velocity in figures). (A) Single trial plots tracing membrane potential, TC excitatory input, RS excitatory input, and FS inhibitory input for a cell within the 0° (left) and 180° (right) directional domains. (B) Single spike raster plots of all cells within the 0° direction domain (left) and 180° direction domain (right) for corresponding trials.

The RS induced current is similar across changing deflection directions. Altering

direction does not alter net activity of the barrel, instead it shifts which groups of cells exhibit

reduced and increased activity. Thus, the homogenous connections (p = 0.2) between all RS cells

throughout the barrel cause comparable net RS current to any given RS cell. However, as velocity decreases, RS induced current tends to decrease as well. Reducing velocity decreases the net number of RS cells spiking within the every direction domain of the barrel. Thus, there is reduced incoming RS current to every RS cell.

TC cells are homogenously synapsed onto FS cells, thus making FS cells similarly responsive for all deflection directions. Thus, FS induced current to the sample RS cells qualitatively does not change as direction changes. However, as velocity is decreased, the FS induced current occurs over a broader temporal scale. As TC spike times desynchronize, dependent FS cell spike times also desynchronize. However, the net spiking activity of FS cells does not vary with velocity.

RS cells within the barrel tend to spike either 0 or 1 times per stimulus (Lee and Simons, 2004; Gabernet et al., 2005; Wilent and Contreras, 2005) because TC excitation has a narrow time window within which a post-synaptic can be initiated before the arrival of potent FS inhibition. In agreement with experimental results, RS cell response rate in the model systematically decreases as velocity decreases (Figure 5A). As velocity decreases, TC spike synchrony decreases, thus fewer TC spikes arrive at the RS synapse within the window of unopposed excitation. Experimentally, RS cells also exhibit systematic decreases in spiking probability as direction of deflection varies toward 180º away from preferred (Bruno and Simons, 2002; Lee and Simons, 2004; Wilent and Contreras, 2005), which is seen in the model (Figure 5B). This occurs as a consequence of low TC → RS synaptic density in high-spiking directional groups. Figure 5C shows the tuning ratio (response to preferred direction/average response over all directions) of a sample RS, TC, and FS cell within the model. In agreement with experimental results, the direction selectivity of RS cells sharpen with decreasing velocity,

while TC cells exhibit a fixed tuning ratio of 1.86, and FS cells are not direction selective (Bruno

and Simons, 2002; Swadlow and Gusev, 2002; Lee and Simons, 2004; Wilent and Contreras,

2005). This sharpening of the RS cell direction occurs because RS cell responses to non-

preferred directions drop more than responses to preferred directions at low velocities (Figure

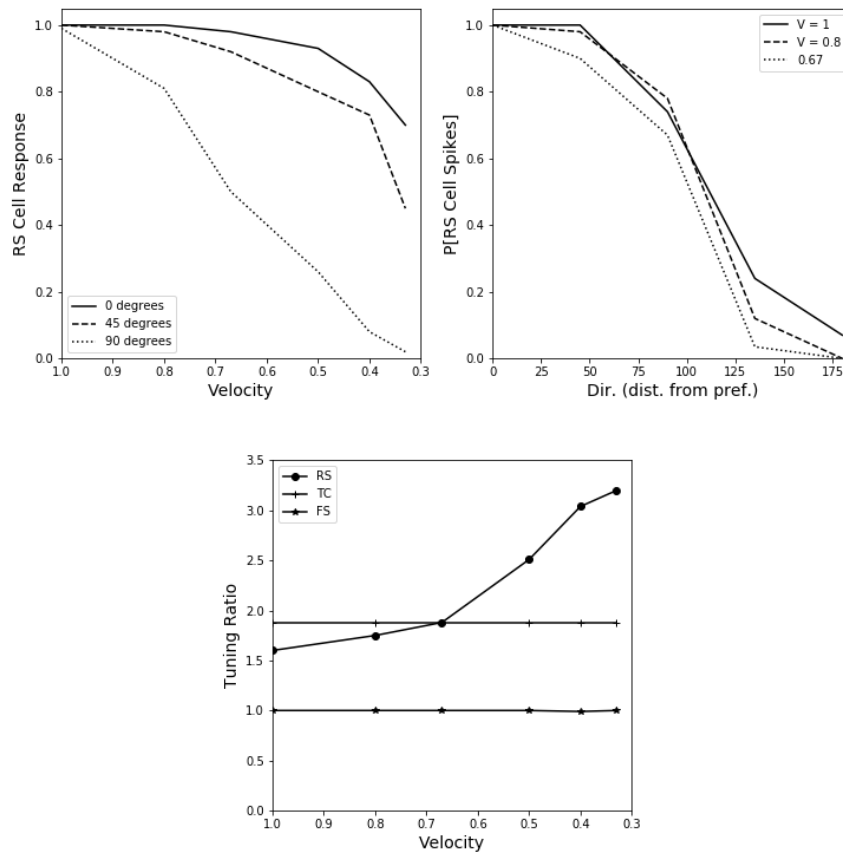5A). These data show that the base model is qualitatively functioning as expected.

Figure 5: (A) Probability that an RS cell spikes versus the velocity of the simulated whisker deflection for three directional groups. Data for 45° and 90° away from preferred are averaged over the ± 45° and ± 90° RS cell groups. (B) Probability that an RS cell spikes versus the direction of simulated deflection (responses averaged over directions equidistant from preferred) for three deflection velocities. (D) Tuning ratio (response to preferred direction/average response over all directions) of the RS cell and a sample TC and FS cell as a function of velocity of deflection.
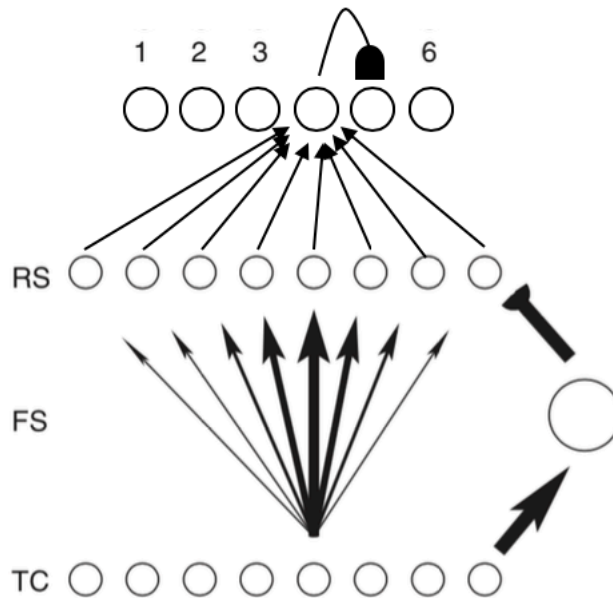
Velocity Disentanglement:

Figure 6: Schematic of the barrel model with an "Excitatory Extension (EE)" layer of RS-like, theoretical cells. Arrow heads indicate excitation while bar heads indicate inhibition. The base model (RS, FS, and TC) layers remain unchanged. All RS cell direction domains synapse with the same probability on every EE cell (p = 0.2). Each of the 6 EE cells will begin responding a specified velocity (6 = 0.33, 5 = 0.4, 4 = 0.5, 3 = 0.67, 2 = 0.8, 1 = 1.0). At spike, each EE cell provides and inhibitory current to the EE cell that responds to the velocity directly below its specified velocity (i.e. the EE cell responding to a velocity of 0.67 inhibits the EE cell responding to a velocity of 0.5).

Velocity information is disentangled from directional information through the addition of a layer of 6 theoretical, RS-like "Excitatory Extension (EE)" cells (see Figure 6). Each of the 6 cells begins spiking at a specified velocity of stimulus. All RS cell direction domains synapse with the same probability on every EE cell, leading to each EE cell having an average of 160 presynaptic RS cell connections. EE cell 1 is arbitrarily assigned to respond to the highest deflection velocity (1), EE cell 2 is assigned to respond to the second highest deflection velocity (0.8) , and so on for all 6 cells. The threshold excitatory input current that must be reached to register an action potential in a particular EE cell is tailored based on which velocity the cell

should respond to. Cell 6 responds to the lowest velocity, and thus has the lowest spike

threshold. Cell 1 is the least responsive of the cells, responding to only the highest velocity, and

thus has the highest spike threshold level. For any given impulse into the system, the final

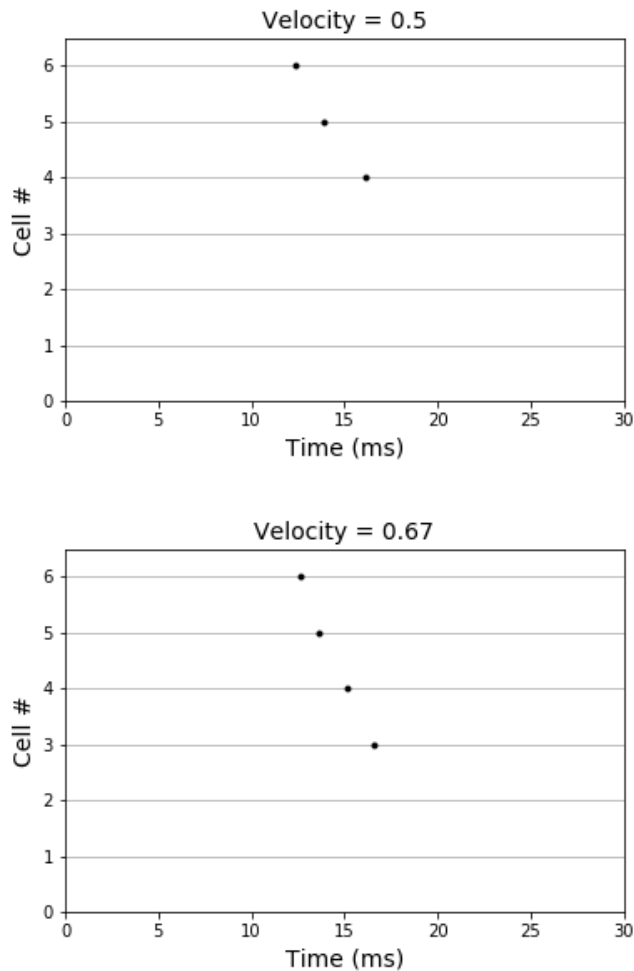velocity is classified as that of the highest velocity EE cell that fired.

Figure 7: Sample raster plots for a velocity of 0.5 and 0.67. (A) For the given input stimulus of 0.5, the system
correctly classifies the velocity. The final classification from the system is based on the highest velocity cell that
fires, cell 4 in this case. Cell 4 corresponds to a velocity of 0.5. (B) For the given input stimulus of 0.67, the system
correctly classifies the velocity based on the spiking of cell 3, which corresponds to a velocity of 0.67.

As velocity increases, increases in TC cell spike synchrony cause net RS cell spiking for

the entire barrel to increase. This increase in net spiking activity is exploited by the model

architecture for use in disentanglement of velocity information. By increasing the spike threshold value for each EE cell by roughly the same proportion by which net RS cell activity increases, velocity-specific cells can be made. However, in this architecture, as seen in Figure 7, the EE cells that respond to lower velocities (EE 6 and EE 5 in Fig. 7A) than the EE cell that finally classifies the input (EE 4 in Fig. 7A) will also spike. These cells (EE 6 and 5 in this example) will also spike at earlier times than the final classification cell (EE 4 in this example). This occurs because of the homogenous distribution of RS $\rightarrow$ EE synapses. The homogenous distribution across the entire RS layer effectively ensures that each EE cell receives roughly the same RS input at any given time. In order for the input current to reach the spike threshold of the final classification cell, it must have reached and surpassed the spike threshold levels needed for the more sensitive classification cells. The effect of the inhibition from one EE cell to the EE cell that classifies the velocity directly below it (i.e. from EE 4 to EE 5) is the curbing of multiple spikes within one EE cell. The inhibition from one cell reaches its post-synaptic target before the target has the opportunity to spike again (either because the cell is still in its latency phase after a spike or has not yet reached threshold). This explains the maximum of one spike for any particular EE cell in Figure 7.
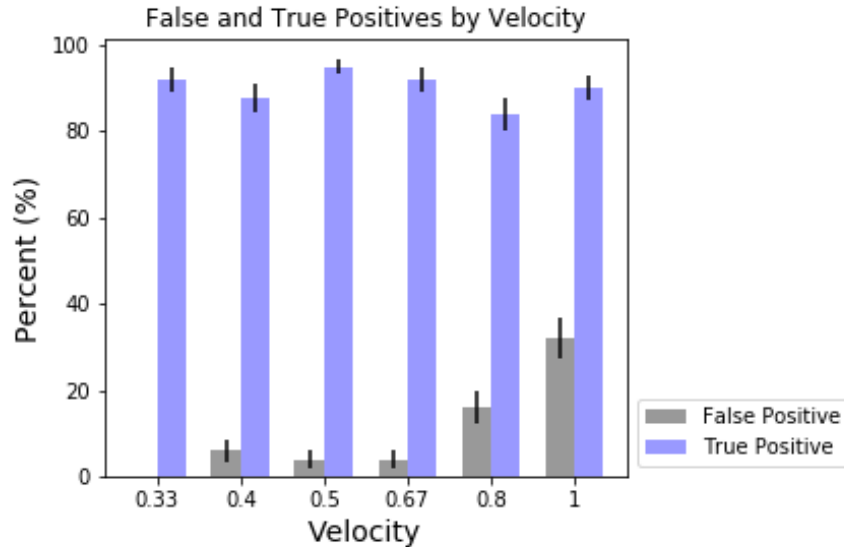
Figure 8: False and true positives presented as percentages with standard error for each velocity-specific EE cell. A false positive is classified as an event when a stimulus as classified as being of a higher velocity than it truly is (in other words, the stimulus velocity excited an EE cell of a higher response than expected. True positives are classified as events when a stimulus velocity is correctly classified by the EE layer.

The percent of false positives (an event where a stimulus is classified as being of a higher velocity than it truly is) and true positives (an event where the stimulus velocity is correctly classified) was calculated for each velocity-tuned EE cell. The percent of true positives for the cells in velocity increasing order ([EE 6, EE 5, EE 4, EE 3, EE 2, EE1]) was found to be [92, 88, 95, 92, 84, 90] with a standard error of [2.7, 3.3, 1.7, 2.7, 3.7 , 2.9]%. The percent of false positives for the cells in velocity increasing order ([EE 6, EE 5, EE 4, EE 3, EE 2, EE1]) was found to be [0, 6, 4, 4, 16, 32] with a standard error of [0, 2.4, 2.0, 2.0, 3.7, 4.7]%. EE 6 has a false positive percent of 0 because by definition of the stimulation, a velocity below 0.33 cannot be provided to the system. This means that the EE cell corresponding to the lowest velocity is expected to spike at every input, which is what is seen. The rate of false positives increases as the velocity increases because RS cell response at any given direction declines more quickly for low velocities than high velocities (Figure 5A). This means that at higher velocities, distinctions between net RS spiking activity for the barrel (what the spike thresholds for the EE cells is based
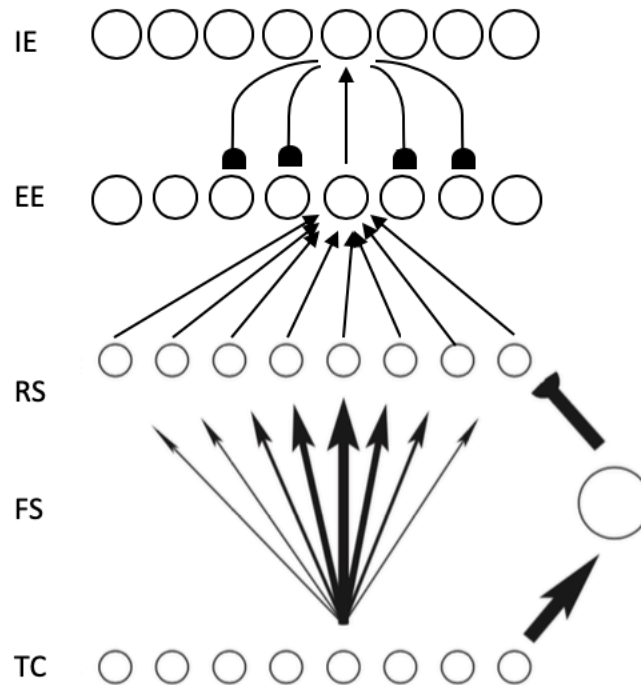
on) is less extreme.

Direction Disentanglement:

Figure 9: Schematic of the barrel model with an additional "Excitatory Extension (EE)" layer and "Inhibitory Extension (IE)" layer of RS-like, theoretical cells. Arrow heads indicate excitation while bar heads indicate inhibition. The base model (RS, FS, and TC) layers remain unchanged. Each of the 8 EE and 8 IE cells correspond to a specific direction. All RS cell direction domains synapse with the same probability on every EE cell (p = 0.2). However, amplitude of current from RS cell to EE cell varies based on directional alignment between RS cell group and EE directional preference. Each EE cell has a corresponding IE cell onto which only it synapses. This IE cell provides inhibitory input to all non-corresponding EE cells upon spiking.

Directional information is disentangled from velocity information through the addition of a layer of 8 theoretical, RS-like "Excitatory Extension (EE)" and 8 theoretical, RS-like "Inhibitory Extension (IE)" cells (see Figure 9). Each of the 8 EE cells corresponds to a specific direction of deflection. Each of the 8 IE cells is assigned an EE cell and forms a pre-synaptic connection with only that cell. Any input from the EE cell will cause an action potential in the corresponding IE cell. The IE cell then provides inhibitory current to all non-corresponding EE

cells. All RS cell direction domains synapse with the same probability on every EE cell, leading to each EE cell having an average of 160 presynaptic RS cell connections. TC cell group 0 is arbitrarily assigned to have a direction corresponding to a 0° difference from the direction of the simulated whisker deflection. Therefore, we RS group 0 and EE cell 0 are also arbitrarily assigned to have a direction corresponding to a 0° difference from the direction of the simulated whisker deflection. Strength of synapses (amplitude of post-synaptic current) increases from RS $\rightarrow$ EE cells as the directional preferences of the groups aligns. For any given simulated whisker deflection stimulus to the system, the final direction is classified as that corresponding to the EE cell that spikes. Every EE cell has relatively the same connectivity as every other EE cell (i.e. the current amplitude for corresponding RS directional groups is equal for every EE-RS pair). Because all directional domains are accounted for within the barreloid (i.e. there are TC groups that correspond to every direction group from 0° to 180°), and the incoming whisker deflection arbitrarily being set to the direction of TC group 0, it will be known if the model architecture correctly disentangles direction information if for every trial, only EE cell 0 spikes.

As TC direction groups align with the direction of the incoming stimulus, the probability that a TC cell within said group increases. This leads to more net TC spiking within groups that are more closely aligned with the incoming input. Because TC cells synapse with preference onto RS cells with similar directional alignment, again, there is more RS spiking within groups of RS cells more closely aligned with the original incoming input. Finally, because RS current amplitudes to its post-synaptic EE cells increase with preference to corresponding directional alignment, EE cells most aligned with the original stimulus have the greatest net excitatory current. Theoretically, this means that in the model, EE cell 0 (corresponding to RS group 0 and TC group 0) should receive the excitatory input needed to cause an action potential most quickly

relative to other EE cells. EE cell 0 will then spike before the other EE cells, and thus the

inhibitory current from its post-synaptic IE cell may reach all other EE cells before they have the

opportunity to spike. This is what is shown in the sample behavior in Figure 10. Only EE cell 0,

corresponding to the greatest net excitatory input through the chain from TC → RS → EE layers,

spikes. This then causes IE 0 to spike, which sends an inhibitory current seen in Figure 10A

shortly after EE0 spikes. This IE inhibitory current provides potent inhibition to all non-

corresponding EE cells, which stops their progression toward threshold.
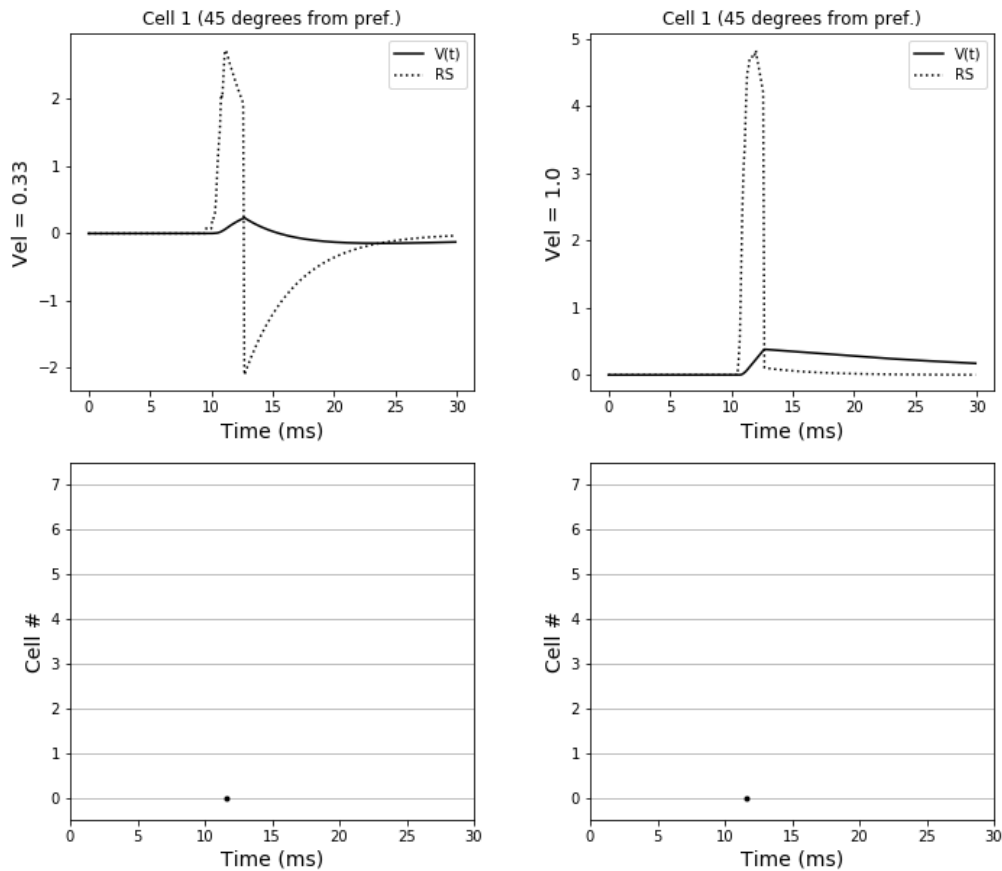

Figure 10: Sample EE cell behavior and single-stimulus raster plots. (A) Single trial plots tracing membrane
potential and RS input for an EE cell 45° away from the direction of simulated whisker deflection for velocity equal
to 0.33 (left) and 1.0 (right). (B) Single spike raster plots for all EE cells during corresponding trials.
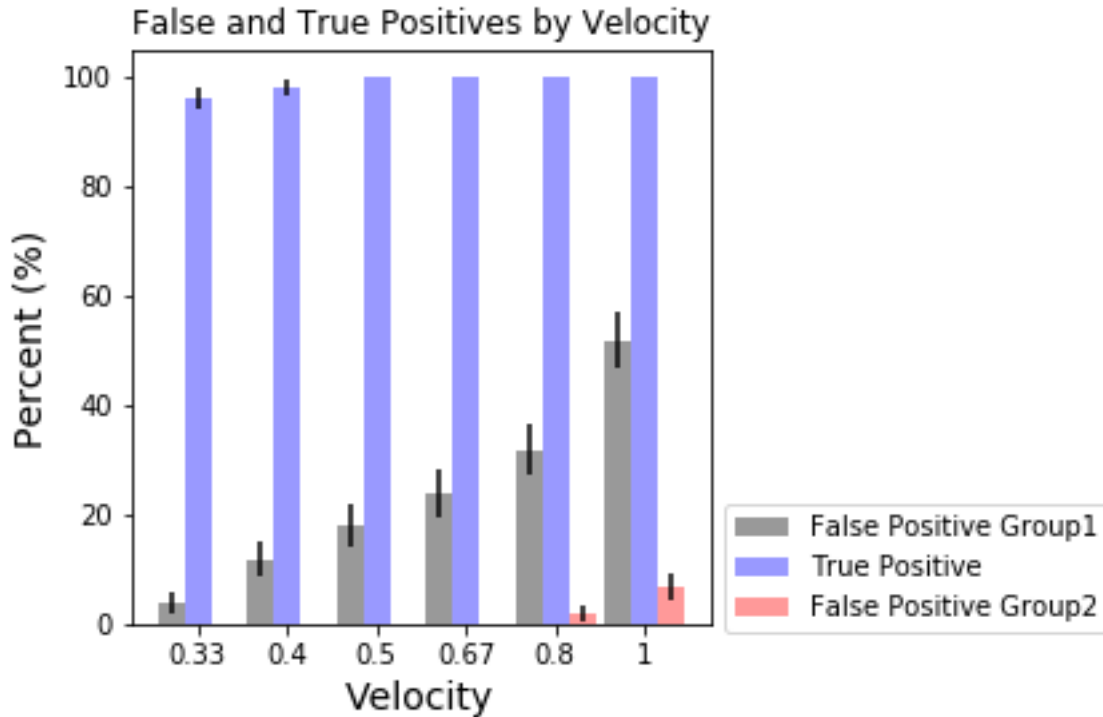
Figure 11: False and true positives presented as percentages with standard error for each direction-specific EE cell. Because choice of TC group corresponding to the direction of the incoming simulated whisker deflection is arbitrary, only EE cell 0 needs to be considered for true positives. A true positive is classified as an event in which EE 0 spikes (even if it is not the only EE cell that spikes). A Group1 false positive is classified as an event where any cell other than the EE 0 cell spikes (even if it is not the only EE cell that spikes). A Group2 false positive is classified as an event where any cell other than the EE 0 or EE 1 and/or EE2 (corresponding to directions +45º and -45º from incoming stimulus, respectively) spikes (even if it is not the only EE cell that spikes).

The percent of group1 false positives (any event where any cell other than the EE 0 cell spikes), group2 false positives (any event where any cell other than EE 0, EE 1, or EE 2 [corresponding to 0º, +45º, and -45º away from incoming stimulus, respectively] spikes), and true positives (any event where EE 0 spikes, even if it is not the only cell to spike) was calculated for the varying velocities. The percentages of true positives for each velocity in increasing order were calculated to be [96, 98, 100, 100, 100, 100] with a standard error of [1.9, 1.4, 0, 0, 0, 0]%. The percentages of group1 false negatives for each velocity in increasing order were calculated

to be [4, 12, 18, 24, 32, 52] with a standard error of [1.9, 3.2, 3.8, 4.2, 4.6, 5.0]%. The percentages of group2 false negatives for each velocity in increasing order were calculated to be [0, 0, 0, 0, 2, 7] with a standard error of [0, 0, 0, 0, 1.4, 2.5]%. The fundamental structure of the architecture is sound, as seen by the high true positive percentages. The cell that corresponds to the direction of incoming current does spike in almost every trial. However, as velocity increases, the tuning ratio of RS cells decreases (Figure 5C). This indicates that RS cells, and thus the EE cells dependent on said RS cells, entangle two close directional inputs more often at higher velocities. Another way to look at the event is by considering the fact that as velocity increases, net RS activity for every directional group increases and becomes more synchronized. This means that the likelihood of EE cell [1-8] spiking before the inhibition from IE 0 arrives at the cell increases.

Conclusion:

The model has shown that with accuracy, a single RS-like cell that classifies velocity without dependency on directional input can be created by taking advantage of the net scaling of RS cell activity with increases in velocity. The model has also shown that a single RS-like cell that accurately classifies direction of simulated whisker deflections without dependency on velocity input can be created using inhibitory feedback. Although the hypothesized cells are not biologically relevant, the mechanisms that affected the desired disentanglement of velocity and directional information may be present within the barrel system. Future areas of study include putting multiple barrel systems in communication (possibly using facets of the architecture developed for the EE cells here) with one another to study whether cells that disentangle these data can be created within the RS layer itself.

References

Arnold P, Li C, Waters R (2001) Thalamocortical arbors extend beyond single cortical barrels: an in vivo intracellular tracing study in rat. Exp Brain Res 136:152–168.

Beaulieu C (1993) Numerical data on neocortical neurons in adult rat, with special reference to the gaba population. Brain Res 609:284–292.

Benowitz L, Karten H (2004) Organization of the tectofugal visual pathway in the pigeon: a retrograde transport study. J Comp Neurol 167:503–520.

Benshalom G, White E (1986) Quantification of thalamocortical synapses with spiny stellate neurons in layer iv of mouse somatosensory cortex. J Comp Neurol 253:303–314.

Blitz D, Regehr W (2005) Timing and specificity of feed-forward inhibition within the LGN. Neuron 45:917–928.

Bruno R (2011) Synchrony in sensation. Curr Opin Neurobiol 21:701–708.

Bruno R, Khatri V, Land P, Simons D (2003) Thalamocortical angular tuning domains within individual barrels of rat somatosensory cortex. J Neurosci 23:9565–9574.

Bruno R, Sakmann B (2006) Cortex is driven by weak but synchronously active thalamocortical synapses. Science 312:1622–1627.

Bruno R, Simons D (2002) Feedforward mechanisms of excitatory and inhibitory cortical receptive fields. J Neurosci 22:10966–10975.

Chen-Bee C, Zhou Y, Jacobs N, Lim B, Frostig R (2012) Whisker Array Functional Representation in Rat Barrel Cortex: Trancendence of One-to-One Topography and its Underlying Mechanism. Frontiers in Neural Circuits 6:93.

Cruikshank S, Lewis T, Connors B (2007) Synaptic basis for intense thalamocortical activation of feedforward inhibitory cells in neocortex. Nat Neurosci 10:462–468.

Deng C, Rogers L (1998) Organisation of the tectorotundal and SP/ IPS-rotundal projections in the chick. J Comp Neurol 394:171–185.

Fox K (2008) *Barrel Cortex*. Cambridge, UK: Cambridge University Press.

Fricker D, Miles R (2000) EPSP amplification and the precision of spike timing in hippocampal neurons. Neuron 28:559–569.

Furuta T, Deschenes M, Kaneko T (2011) Anisotropic distribution of thalamocortical boutons in barrels. J Neurosci 31:6432–6439. Gabernet L, Jadhav S, Feldman D, Carandini M, Scanzianiemail M

Jensen K, Killackey H (1987) Terminal arbors of axons projecting to the somatosensory cortex of the adult rat. I. The normal morphology of specific thalamocortical afferents. J Neurosci 7:3529–3543.

Jortner R, Farivar S, Laurent G (2007) A simple connectivity scheme for sparse coding in an olfactory system. J Neurosci 27:1659–1669.

Joshi B, Patel M (2013) Encoding with synchrony: phase-delayed inhibition allows for reliable and specific stimulus detection. J Theor Biol 328:26–32.

Kawaguchi Y, Kubota Y (1993) Correlation of physiological subgroupings of nonpyramidal cells with parvalbumin- and calbindind28k-immunoreactive neurons in layer v of rat frontal cortex. J Neurophysiol 70:387–396.

Keller A, Carlson G (1999) Neonatal whisker clipping alters intracortical, but not thalamocortical projections, in rat barrel cortex. J Comp Neurol 412:93–94.

Land P, Buffer S, Yaskosky J (1995) Barreloids in adult rat thalamus: three dimensional architecture and relationship to somatosensory cortical barrels. J Comp Neurol 355:573–588.

Lee S, Simons D (2004) Angular tuning and velocity sensitivity in different neuron classes within layer 4 of rat barrel cortex. J Neurophysiol 91:223–229.

Leitch B, Laurent G (1996) GABAergic synapses in the antennal lobe and mushroom body of the locust olfactory system. J Comp Neurol 372:487–514.

Liu R, Patel M, Joshi B (2014) Encoding whisker deflection velocity within the rodent barrel cortex using phase-delayed inhibition. J Comput Neurosci 37:387–401.

Lubke J, Egger V, Sakmann B, Feldmeyer D (2000) Columnar organization of dendrites and axons of single and synaptically coupled excitatory spiny neurons in layer 4 of the rat barrel cortex. J Neurosci 20:5300–5311.

Mittmann W, Koch U, Ha¨usser M (2005) Feed-forward inhibition shapes the spike output of cerebellar purkinje cells. J Physiol 563:369–378.

Patel M, Reed M (2013) Stimulus encoding within the barn owl optic tectum using gamma oscillations vs. spike rate: a modeling approach. Netw Comput Neural Syst:52–74.

Patel, M (2018) Spiking and Excitatory/Inhibitory Input Dynamics of Barrel Cells in Response to Whisker Deflections of Varying Velocity and Angular Direction. Neuroscience 369: 15–28.

Perez-Orive J, Mazor O, Turner G, Cassenaer S, Wilson R, Laurent G (2002) Oscillations and sparsening of odor representations in the mushroom body. Science 297:359–365.

Petersen C (2007) The functional organization of the barrel cortex. Neuron 56:339–355.

Pinto D, Brumberg J, Simons D (2000) Circuit dynamics and coding strategies in rodent somatosensory cortex. J Neurophysiol 83:1158–1166.

Pinto D, Hartings J, Brumberg J, Simons D (2003) Cortical damping: analysis of thalamocortical response transformations in rodent barrel cortex. Cereb Cortex 13:33–44.

Pouille F, Scanziani M (2001) Enforcement of temporal fidelity in pyramidal cells by somatic feed-forward inhibition. Science 293:1159–1163.

Simons D, Carvell G (1989) Thalamocortical response transformation in the rat vibrissa/barrel system. J Neurophysiol 61:311–330.

Sridharan D, Boahen K, Knudsen E (2011) Space coding by gamma oscillations in the barn owl optic tectum. J Neurophysiol 105:2005–2017.

Sun Q, Huguenard J, Prince D (2006) Barrel cortex microcircuits: thalamocortical feedforward inhibition in spiny stellate cells is mediated by a small number of fast-spiking interneurons. J Neurosci 26:1219–1230.

Swadlow H, Gusev A (2002) Receptive-field construction in cortical inhibitory interneurons. Nat Neurosci 5:403–404.

Tao L, Shelley M, McLaughlin D, Shapley R (2004) An egalitarian network model for the emergence of simple and complex cells in visual cortex. Proc Natl Acad Sci USA 101:366.

Temereanca S, Brown E, Simons D (2008) Rapid changes in thalamic firing synchrony during repetitive whisker stimulation. J Neurosci 28:11153–11164.

Temereanca S, Simons D (2003) Local field potentials and the encoding of whisker deflections by population firing synchrony in thalamic barreloids. J Neurophysiol 89:2137–2145.

Timofeeva E, Merette C, Emond C, Lavallee P, Deschenes M (2003) A map of angular tuning preference in thalamic barreloids. J Neurosci 23:10717–10723.

Wehr M, Zador A (2003) Balanced inhibition underlies tuning and sharpens spike timing in auditory cortex. Nat 426:442–446.

Welker C, Woolsey T (1974) Structure of layer iv in the somatosensory neocortex of the rat: description and comparison with the mouse. J Comp Neurol 158:437–453.

Wilent W, Contreras D (2005) Dynamics of excitation and inhibition underlying stimulus selectivity in rat somatosensory cortex. Nat Neurosci 8:1364–1370.

Woolsey T, Van der Loos H (2000) The structural organization of layer IV in the somatosensory region (SI) of mouse cerebral cortex. The description of a cortical field composed of discrete cytoarchitectonic units. Brain Res. 17(2): 205–242.